AN ABSTRACT OF THE THESIS OF

Alan Thomas Grier for the degree of Master of Science in Mechanical Engineering presented on May 30, 2019.

Title: Automated Tradeoff Analysis of Cost Versus Machinability for Design Feedback

Abstract approved: _____

Matthew I. Campbell

As CAD tools become more sophisticated, engineers are able to more easily create complex part geometries with minimal mass given strength and stiffness requirements. However, these complex part geometries can be difficult to subtractively manufacture, which consequently increases manufacturing cost and production time. This thesis presents a method independent of CAD kernels for use early in the design process to automatically evaluate a given part's machinability and to provide visual geometric additions that decrease manufacturing cost while maintaining the part's strength and stiffness requirements. Slicing a single part into multiple sub-parts, which are joined together after undergoing pre-machining, offers additional possibilities for cost reduction and machinability improvement by utilizing smaller stock material that requires fewer machining operations. The resulting part geometry for each candidate is determined by intersecting the machinable geometries for each individual machine setup, and may have some amount of added volume over the as-designed part. Evaluating and culling candidates

based on two objectives (added volume and cost) provides the design engineer with a set of Pareto-optimal solutions that show where material can be added to reduce manufacturing costs. These methods are implemented and tested on five example parts to demonstrate their capability and utility.

Automated Tradeoff Analysis of Cost Versus Machinability for Design Feedback

by

Alan Thomas Grier

A THESIS

submitted to

Oregon State University

in partial fulfillment of
the requirements for the
degree of

Master of Science

Presented May 30, 2019
Commencement June 2019

Master of Science thesis of Alan Thomas Grier presented on May 30, 2019.

APPROVED:

Major Professor, representing Mechanical Engineering

Head of the School of Mechanical, Industrial, and Manufacturing Engineering

---

Dean of the Graduate School

I understand that my thesis will become part of the permanent collection of Oregon State University libraries. My signature below authorizes release of my thesis to any reader upon request.

Alan Thomas Grier, Author

ACKNOWLEDGEMENTS

I would like to thank my advisor, Prof. Matt Campbell, as well as Dr. Brandon Massoni for their support and and mentorship throughout my development of this thesis. Additionally, thanks are also due to Profs. Karl Haapala, Bob Paasch, and Wade Marcum for serving on my thesis committee and providing feedback on my thesis.

I would also like to thank the Boeing Company and the Oregon Metal Initiative (OMI) for their financial support for work leading up to this project. Views expressed in this thesis are my own, and do not reflect the opinions of these supporters.

I would like to acknowledge several of my peers for their support in providing valuable feedback on my ideas throughout this process: Connor Torris, Sam Nicholson, Nate Rust, John Kittelman, Brad Anderson, and Kyle O'Brien.

Lastly, I would like to thank the rest of my family and friends–especially my parents Carla and David Grier–for their continuous help, listening, and thought whenever I've needed it.

TABLE OF CONTENTS

TABLE OF CONTENTS (Continued)

LIST OF FIGURES

LIST OF FIGURES (Continued)

LIST OF FIGURES (Continued)

LIST OF FIGURES (Continued)

LIST OF TABLES

Chapter 1: Introduction

Computational design tools are enabling engineers to design ever more intricate and organic part geometries, while not being met with similar advancements for how these parts will be manufactured. Indeed, advances in manufacturing afforded by 3D printing allow for complex geometries that are in some ways difficult to design, but the connection between how a part is designed and how it is manufactured appears to have diverged. While additive technologies are now prevalent, production scale and time requirements still necessitate manufacturing a majority of commercial products with traditional subtractive methods (e.g. milling and turning). This rift between design tools and manufacturing capabilities increases time spent by the engineers ensuring parts are manufacturable.

The design engineer needs rapid, automated feedback to know if the parts they are designing are machinable, and roughly how expensive they will be to machine. They can then explore different design tradeoffs to improve machinability and decrease part cost. This is especially useful when designers employ topology optimization techniques[1] and use other automated design tools that lack consideration of how a part will be manufactured. An example topology optimized (Fig. 1.1) part is impossible to machine exactly as designed and does it allow for further material removal, but can be machined to within 9% of designed mass with only three machine setups on a three-axis milling machine.

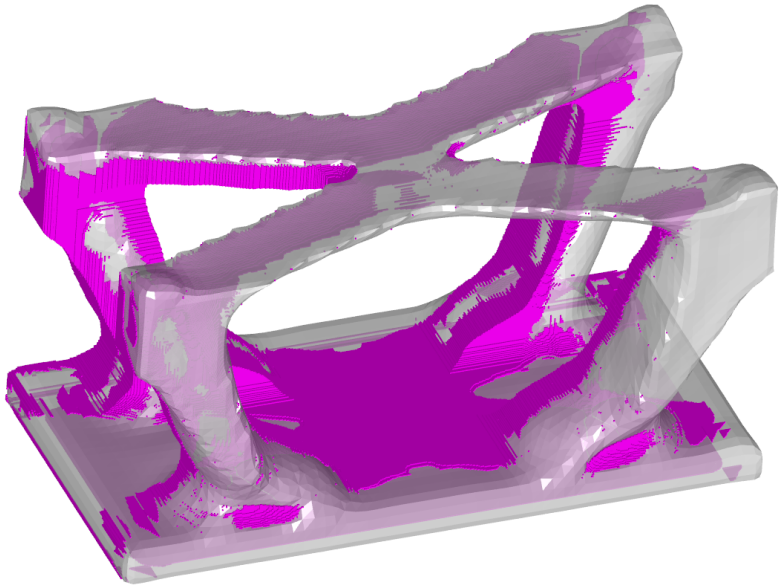

Figure 1.1: Topology optimized part (light grey, translucent) that cannot be fully machined by traditional methods. Minimum material left after machining with only three setups (9% added volume) shown overlayed (magenta).

In cases where the engineer cannot compromise on added volume, utilizing cutting planes to slice a part into multiple sub-parts is a valuable technique to improve machinability. A few benefits of slicing a part into smaller sub-parts include exposing previously unmachinable regions, reducing the number of required machining setups, and potentially decreasing manufacturing cost. Sub-parts can be be machined individually, after they are joined together, or a combination of both. The example part shown in Fig. 1.2 is approximately 17% less expensive to manufacture from two sub-parts which are joined together, and still serves the original purpose as intended by the engineer. This cost reduction is primarily a result of the significant decrease in stock material, which in turn decreases the required amount of machining (i.e. material waste). The results

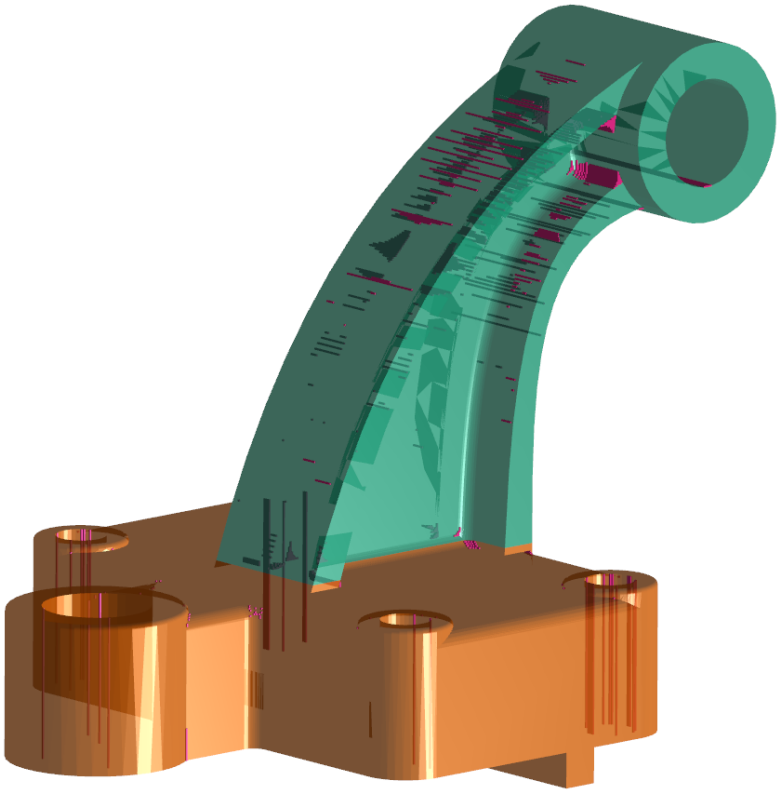

Figure 1.2: Prismatic part with a large void area within its bounding volume. Slicing the part in two and pre-machining each sub-part allows for a cost reduction of nearly 17%. The two sub-parts can then be joined together afterwards, and any post-processing performed on the part as a whole.

shown with these parts demonstrate several of the many findings made possible by the developed research presented here.

Our presented methods are intended for use early in the design process to give the design engineer machinability and cost feedback with far less interaction than what is required by traditional computer aided machining (CAM) or costing software. This tool provides engineers with alternative designs and the difference in cost associated with those and the as-designed part. Once the designer is satisfied with the evaluated machin-

ability and estimated cost, the part can be analyzed with more advanced costing tools or signed off to manufacturing.

Chapter 2: Literature Review

There has been considerable research performed on both manufacturing feasibility and cost estimation, but little research considers these areas simultaneously. This chapter presents an overview of relevant research in these areas, as well as how it differs from the new research presented in this thesis.

2.1 Manufacturability Analysis

Similar work is presented by Hoefer et al.[2], which also develops a software tool (ANA) for manufacturability analysis. Their tool returns a machinability "score" based on four basic criteria–visibility, reachability, accessibility, and setup complexity–and plots that score for different regions of a part as a heat–map over the geometry. Kim et al.[3] propose a methodology for analyzing a part's manufacturability with a set of heuristic filters, and then identifying suitable manufacturing processes.

An early example of voxel-based machinability is presented by Jang et al.[4], who developed a simulation to visualize and validate complicated CNC toolpaths. The use of voxels allows them to easily estimate material removal rate and subsequently adjust feedrate and spindle speed to optimal parameters. Frank et al.[5, 6] present methods for estimating a part's machinability and required setup orientations by slicing a part along numerous axes and performing a series of polygonal operations.

Several researchers have demonstrated the usefulness of visibility cones[7, 8] for automating design for manufacture. Their applications include efficiently planning setups for 3, 4, and 5-axis milling machines, as well as evaluating machinability and informing the design of unmanufacturable regions.

Early work in the field by Chu et al.[9] classifies geometric features into two categories: single tool approach direction (STAD) and multiple tool approach direction (MTAD). Machine setups are created for all STAD features, with additional setups added as needed for MTAD features which cannot use any of the STAD setups. Research performed by Ong et al.[10] seeks to develop a set of methods to evaluate a part's machinability and fixturability using fuzzy set theory and an analytical hierarchy process. To much the same effect, Fu et al.[11] decompose parts into Boolean subvolumes (which can be either machined or not) and apply graph grammar rules to determine a suitable machining plan and holding fixture.

Related work carried out by Nelaturi et al.[12, 13] provide a method for determining machining plans of an arbitrary part geometry. Their work also automatically creates a modular fixture which ensure both form and force closure, and does not interfere with the machining operations. Behandish et al.[14] expand further on these ideas with the software tool, uFab. This software performs tool-path planning to provide cost estimates and help engineers improve their skills in design for manufacture.

Prior research performed within our current lab by Chan et al.[15] have already developed voxel-based methods for estimating machinability of arbitrary part geometries, although limited to setups aligned with a part's datum axes. The example topology optimized part (Fig. 1.1) is borrowed from the results of research performed by Mirzen-

dehdel et al.[16] on multi-objective (seeking to minimize mass and compliance) and multi-material topology optimization.

Jared et al.[17] examine how geometric reasoning can be used to efficiently transfer solid model data to generic design for assembly tools. In their sweeping review of manufacturability analysis systems, Gupta et al.[18] study numerous methods for assembly planning and component machinability. They characterize different benefits and shortcomings of all those manufacturability analyses. The research presented in this thesis provides an accurate evaluation of component machinability for parts manufactured on 3-axis milling machines, and provides geometric feedback for how to improve part machinability.

2.2 Cost Estimation

Early research conducted by Corbett et al.[19] resulted in a computerized database with cost models for different manufacturing processes and materials, including labor and tooling. This was intended for early in the design process, but its usage required entirely manual input of geometric parameters. Boothroyd et al.[20] helped pioneer the development of early-design process cost estimation for different manufacturing methods. Their methods allowed for cost manufacturing cost estimates without developing a machining plan or toolpaths.

Geiger et al.[21] present an automated “design-to-cost” system which estimates the cost for a given part, and then searches a database for similar parts with a different cost. Information relating to the part’s geometry is manually entered into the system through

a text interface. Work performed by Jung[22] sought to provide engineers with a cost estimation for manufactured features using cost models for several basic machining operations. More complex features are characterized by some number of these simpler operations.

A software tool developed by Das et al.[23], Pro-DFM is capable of analyzing the manufacturing feasibility of new products according to three basic criteria: part procurement, manufacturing and assembly processes, and inventory cost. The industry tool, aPriori[24, 25], provides design engineers with precise cost estimates to evaluate different designs against each other. High accuracy comes at the expense of requiring the engineer to ensure machinability before costing, making aPriori useful later in the design process. Our research aims to provide an early design-process machinability and cost estimation tool that is capable of suggesting specific design changes to decrease part cost.

Related work within our lab by Massoni et al.[26, 27] suggest decomposing complex parts into pre-machined subparts that are joined together by friction welding. Massoni et al. then define and solve an optimization problem to find the minimum cost solution for how to divide the part and then join the sub-parts together. The presented research expands the available voxel operations and applies a similar optimization process to the machining plan of single parts and multiple sub-parts that are joined together.

Chapter 3: Methodology for Single Part Machinability Analysis

The approach developed and described hereafter aims to assist the design engineer in evaluating a part's machinability and identifying tradeoffs between machinability and cost. These tradeoffs are presented to the engineer as Pareto plots comparing added volume and cost. Each point on the Pareto plot represents a compromise wherein additional material is left unmachined on the as-designed part. This added material is shown in a contrasting color to inform the user of where material could be added to reduce cost. Reflecting on the added materials informs the user on what modifications can be made to reduce part cost.

The high-level process requires the engineer to first produce a tessellated geometry file from their CAD tool (e.g. ".STL", ".PLY", ".3MF"). Within our developed computational process, the part is voxelized and machine setup directions are determined. A search tree is used to select the best subsets of machining directions that minimize cost and deviation from the original as-design shape. Operations relating to the tessellated parts and voxelization are performed using Tessellation and Voxelization Geometry Library (TVGL)[28].

3.1 Defining Part Volume

In this research, parts are assumed to be manufactured with conventional milling out of rectangular stock sized to the part. Stock is oriented with the part's minimum enclosed-volume bounding box (also known as the oriented bounding box, or OBB[29]), and it is assumed that the part can be fixtured for milling from any direction. It is important to note that the OBB may not always align the primary datums the part has been designed around, especially for parts which are long and narrow. Although the OBB will be rotated from the part's primary axes in such circumstances, this does not affect the machinability algorithm.

3.2 Finding Search Directions

Parts intended for machining with traditional 3-axis milling are often designed to only require setups corresponding to their own primary datums, or cardinal axes–that is machining from +X, +Y, +Z, -X, -Y, and -Z. Functionality requirements may, however, necessitate features such as holes that are not aligned with a part's cardinal axes, or a part has been topology optimized and has no clear cardinal directions. For these cases, it is necessary to consider additional machining setups beyond the part's cardinal axes. It is important to note that–if a new machining axis is found–it may be important to consider the positive and negative directions along that axis independently.

To address this, the input tessellated part geometry is taken and decomposed into various shape primitive, such as cylinders, cones, flats, spheres, and tori. Previous efforts by the lab were able to find these primitives within tessellated meshes[30]. We assume

that cylinders provide the key to finding useful off-axis directions. In particular, negative or internal cylinders that would correspond to drilled holes or filleted sections. Certain criteria for consideration include a minimum radius and either a minimum surfaces area or number of cylinders sharing the same direction. The minimum radius and surface area are normalized by the overall part size to create a dimensionless scale unaffected by part size. Improvements may be made to this approach, which are discussed in Chapter 7.

3.3 Search Tree

The search is multi-objective in nature, weighing part volume against cost, and seeking to minimize both objectives. For some number (n) of potential machine setup directions, each setup will either be used or not used for any combination of setups. This results in 2^n possible combinations of machining setups and an exponential increase in time required to evaluate all solutions. Evaluating the solution containing no machine setups is trivial, and the the effective space size, N, reduces by one (given in Eq. (3.1)). A multi-start implicitly-enumerated tree search selectively searches the space of machine setup combinations.

$$N = 2^n - 1 \tag{3.1}$$

An initial tree search is performed for machine setups aligned with the six cardinal axes. Starting with a state of no machining, each of the six directions create six successor states. From these, we add the subsequent machine setups, creating up to 63 (2^6-1) initial

solutions (ignoring that where no machining is performed). This is akin to a breadth first search. An arbitrary state (of two operations: +X, -Y) and selected child solutions are shown in Fig. 3.1. As the search progresses, poorly performing solutions–those which do not decrease the volume objective–are immediately discarded and their successor states will not be created. Once a certain combination of setups is deemed unhelpful, later states containing those same machine setups will be immediately discarded prior to machinability evaluation. These two space reduction methods are demonstrated in Fig. 3.1, which includes a candidate state (+X, -Y, and -Z) that does not reduce the amount of added volume; thus, it is deleted. A completely different candidate (with states +X, -Y, and +Z) will now be prevented from adding -Z as this would fulfill a combination that is now unproductive.

The second stage of the implicitly-enumerated tree search incorporates the prior identified off-axis machine setup directions. All solutions from the first search–including the state where no machining has been performed) form an initial set of states to implicitly enumerate candidates with each off-axis direction. The same space reduction techniques employed in the first stage are used here.

3.4 Machining Cost Objective

The cost (C_m, Eqs. (3.2) and (3.3)) for any given candidate can be determined at different accuracy with varying amounts of process information. Knowing the volume to be machined away (V_{mach}), material removal rate (MRR), and the cost-rate for machine time (C_r) is sufficient, but the cost estimate can be made more accurate if more process-

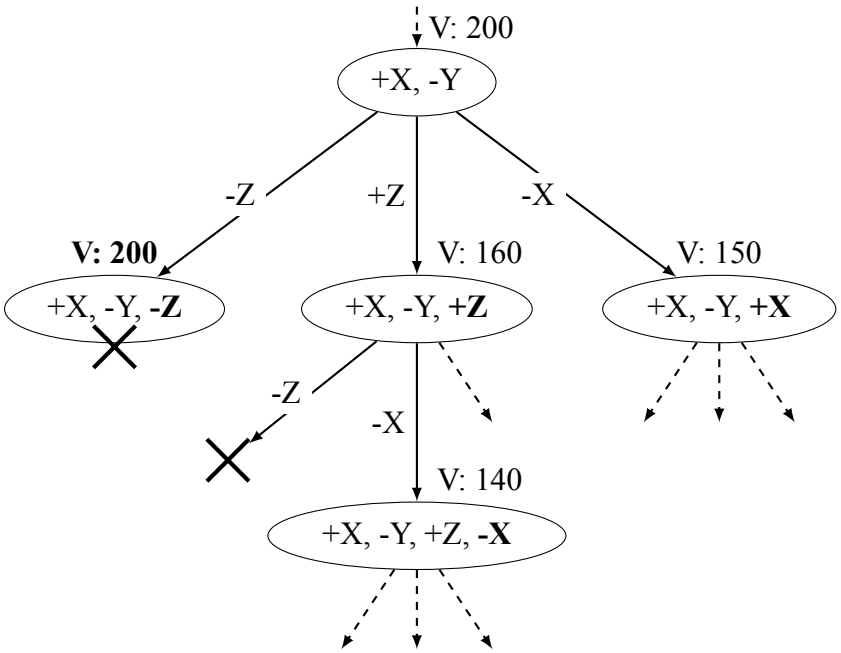

Figure 3.1: Section of exhaustive search tree showing search space reduction techniques. Solutions providing no reduction in volume (+X, -Y, -Z) are discarded, and later candidates containing the same combination of setups (+X, -Y, +Z, -Z) are discarded before evaluation.

specific and machine-specific information is made available. Incorporating part setup and removal time (T_s) significantly improves the cost estimate, as the number of unique machining setups can be factored in. Other useful parameters include tool cost and life, as well as the amount of finish machining needed. Tool cost and life are simple to include so long as they are known, and the required time for finish machining can be estimated based on the surface area of the machined part.

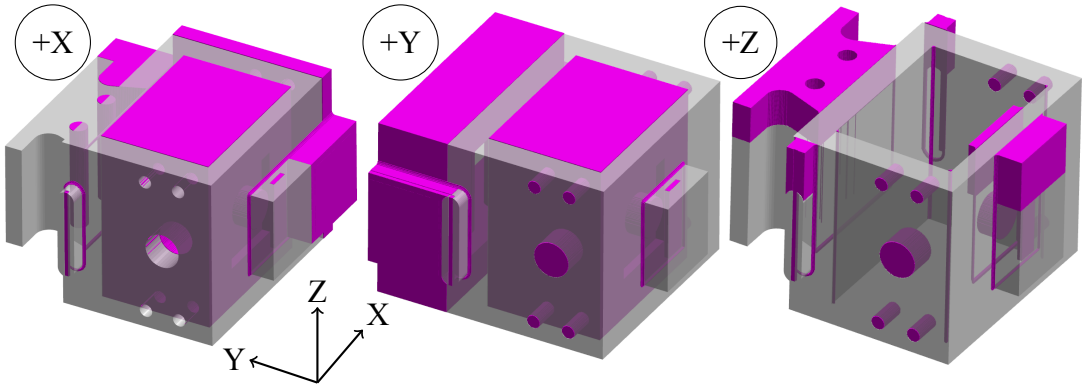

Figure 3.2: Maximum machinable solids for test part A using machine setups in positive X, positive Y, and positive Z.

$$C_m = C_r \times (T_m + T_s) \tag{3.2}$$

$$T_m = \frac{V_{\text{mach}}}{\text{MRR}} \tag{3.3}$$

3.5 Voxel Operations

The process of evaluating each candidate solution involves building a set of maximum machinable shapes (MMS)–one for each direction the part can be machined from. Each MMS represents the part geometry after the maximum amount of machining for any single setup is performed. A small example set of these are shown in Fig. 3.2. For any combination of setup directions, the corresponding MMSs can be intersected together to produce the resultant solid of machining with those setups. The user-input tessellated geometry is voxelized and a voxel solid representing the OBB is also created.

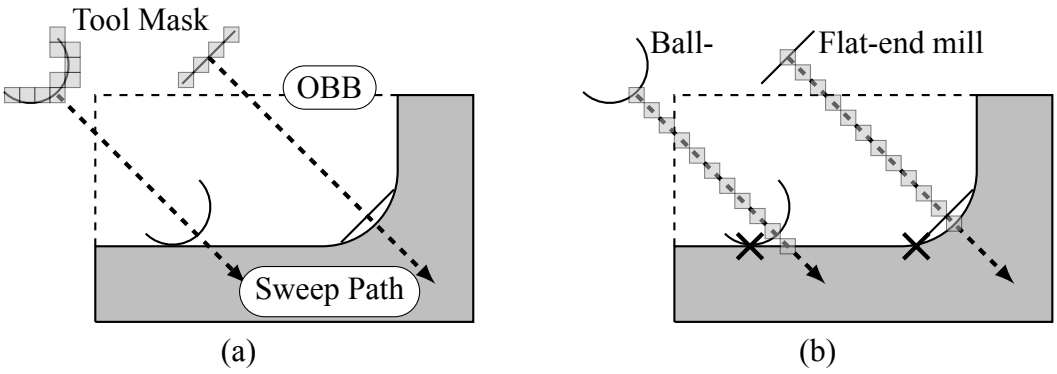

Figure 3.3: 2D cross section of a part and its OBB. Voxel masks for ball and flat end mills are shown in (a). Sweep path voxelization and terminal location of sweep (marked by "X") are shown in (b).

The method presented by Chan et al.[15] drafts the designed solid in each direction, adding voxels until arriving at the representation of what is machinable in each direction. Considering tool diameter and end condition–flat, ball, et cetera–leads to a method much more analogous to physically machining a part. Voxels that the tool would be able to reach are removed from the OBB until the resultant solid for each machining setup is reached. This is achieved by repeatedly sweeping the tool from different starting locations through the OBB until the tool collides with the designed solid.

Several different voxel masks are created to aid in this process, beginning with the *tool mask*. The leading surface of the tool is represented by a set of voxel coordinates that are relative to the leading point (front center) of the tool. These coordinates correspond to either a disc of voxels or hemisphere of voxels for a flat or ball end mill, respectively (Fig. 3.3a). The orientation of the tool relative to the part–based on machine setup direction–is also accounted for during creation of this mask.

A *sweep path* defines the sequence of corresponding coordinates for all voxels the leading point of the tool intersects on a single sweep, relative to any arbitrary starting voxel of a sweep. This is shown in Fig. 3.3b. All OBB voxels that the *tool mask* passes through are removed. Each sweep concludes when any voxel in the *tool mask* intersects with a voxel belonging to the designed solid. This is shown by the "X" in the figure. The process is repeated using this same sweep path direction for all possible starting locations outside of the solid.

The resulting voxel solid (MMS) for a given machine setup is the union of the designed part and the unmachinable geometry for that setup. Different combinations of MMS are intersected to form the resultant geometry for the corresponding set of machine setups. The amount of added volume for each is calculated as the difference in volumes for the given MMS (or intersect of multiple MMSs) and the designed solid, while the cost calculation makes use of the material volume removed for each MMS or intersected solid.

Different resolutions of voxelization are shown in Figure 5 and required time, memory, and voxelization error are tabulated in Table 1. For a prismatic part (A, Fig. 4.1), there is a roughly linear decrease in volume error with increases in voxel resolution. Similar resolution changes of a topology optimized part (C) yield diminishing reduction of error compared to the greater increase in required computational time. These tests were run on a workstation with 32 GB DDR4 memory and a 4-core (8-thread) processor clocked at 3.7 GHz.

Table 3.1: Comparison of required time and memory for a single-setup machinability analysis and voxelization error relative to the tessellated part at different voxel resolutions for Parts “A” and “C”.

Voxels on Longest Side	**Volume [% Error]**		**Time [s]**		**Memory [MiB]**	
	A	C	A	C	A	C
128	0.58	2.89	0.37	0.29	59	88
256	0.28	0.24	0.61	1.48	104	109
512	0.18	0.36	8.56	28.7	379	234
1024	0.06	0.16	236	866	1580	1040

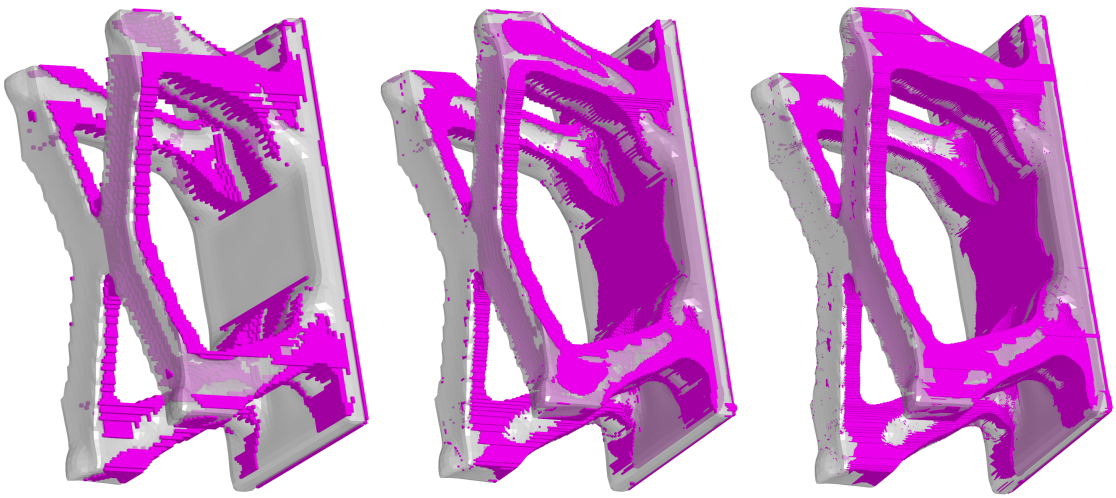

Figure 3.4: Comparison of two-setup machinability analysis for different resolutions of voxelized Part C. From left to right, solids have 128, 256, and 512 voxels along their longest side. This part’s bottom side features a large, concave surface that is only captured by resolutions of 256 and greater.

Chapter 4: Results for Single Part Machinability Analysis

This chapter presents an application of the described methodology to a set of three sample parts using two different tool styles. The experiment uses a ten-millimeter diameter end mill with both flat and ball geometries, yielding six distinct experiments. Material is assumed to be titanium, and parts smaller than 2.5 kg are chosen such that small machines can be used. A roughing MRR of 50 cm^3 per minute is used, and the finishing MRR is assumed to be 5 cm^3 per minute. Machine setup time is estimated to be 60 minutes. A load/unload time of 10 minutes per setup is used, and the machine cost-rate is estimated at $60 per hour. Tool life and cost are estimated to be 90 minutes and $200, respectively. All three parts are of roughly same length scale, having minimum and maximum dimensions varying from 80 millimeters to 370 millimeters.

Shown in Fig. 4.1, each part exhibits unique geometry features that test the proposed methods under various machining scenarios. Part A features a large internal void with protrusions in several different directions, as well as a small pocket which cannot be machined due to the overhang above it. Part B includes holes not aligned with the part's cardinal axes. Part C is the result of a computer-aided topology optimization and has few prismatic features.

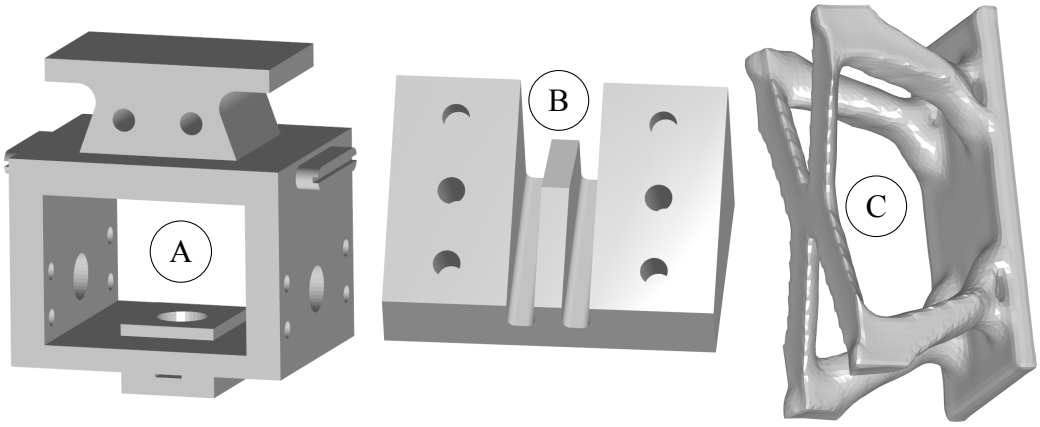

Figure 4.1: Machinability test parts. A contains unmachinable regions; B contains off-axis features; C is a product of topology optimization.

4.1 Prismatic: Part A

Inspecting the results for part A, the Pareto plot–shown in Fig. 4.2–has five key regions. Starting from the bottom right where points have high added volume (AV) and low cost, there appears to be a linear trend (shown at the circled 1 in Fig. 4.2) until several additional setups significantly increase the cost with little reduction in AV (at 2 in the figure). There is then a large decrease in AV with little change in cost (3 in the figure) to a point where solutions follow the original linear trend (4 in the figure). Near the cost axis, the Pareto front ends with additional setups providing little decrease in AV (5 in the figure).

By zooming in on this region (as shown in Fig. 4.3), we notice that the most machinable solution still has nearly one percent AV. This is result of the part having a blind hole that cannot be reached by a traditional milling tool. Three Pareto-optimal solutions near points “2”, “3”, and “4” are shown in Fig. 4.4. Throughout the plot, we can see that there is not significant difference between ball-end and flat-end mills. In comparing the

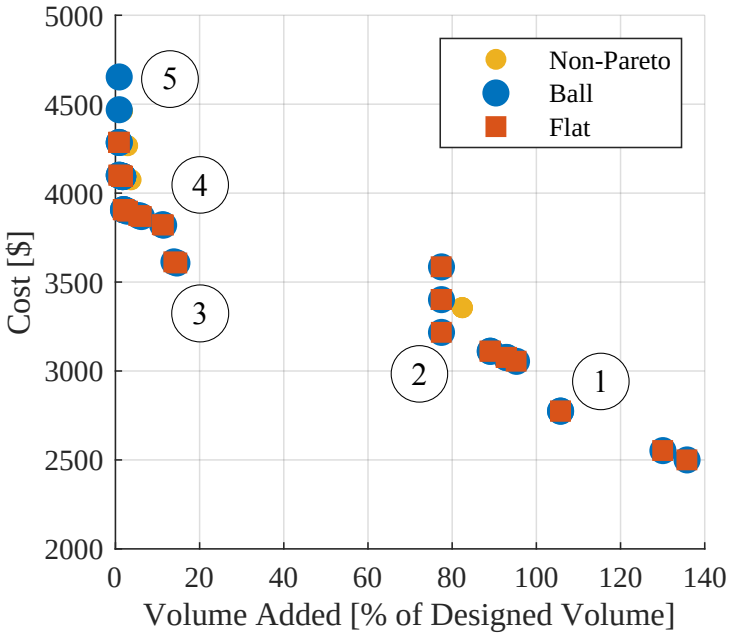

Figure 4.2: Pareto plot for Part A. 1: Linear increase in cost with reduced AV. 2: Increase in cost with no change to AV. 3: Large decrease in AV with no change to cost. 4: Co-linear with (1). 5: Increase in cost with little change to AV.

same combination of machine setups with both tool types (shown in Fig. 4.5), using a flat end mill results in slightly improved machinability over a ball end mill. Fewer fillets are leftover by the flat-bottomed tool where multiple setups expose the same concave edges.

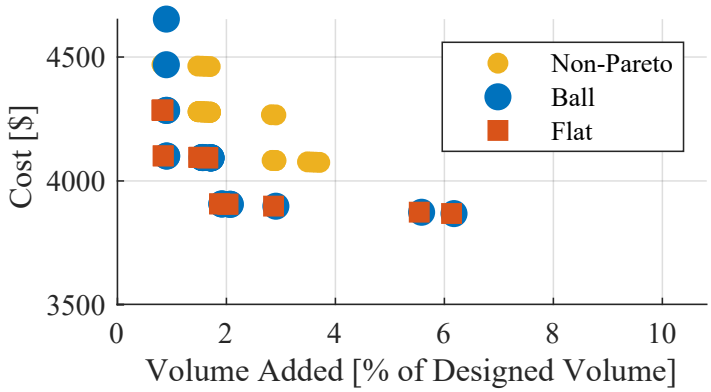

Figure 4.3: Reduced domain (0% to 10%) Pareto plot for Part A, showing non-zero minimum AV as a result of an unmachinable region.

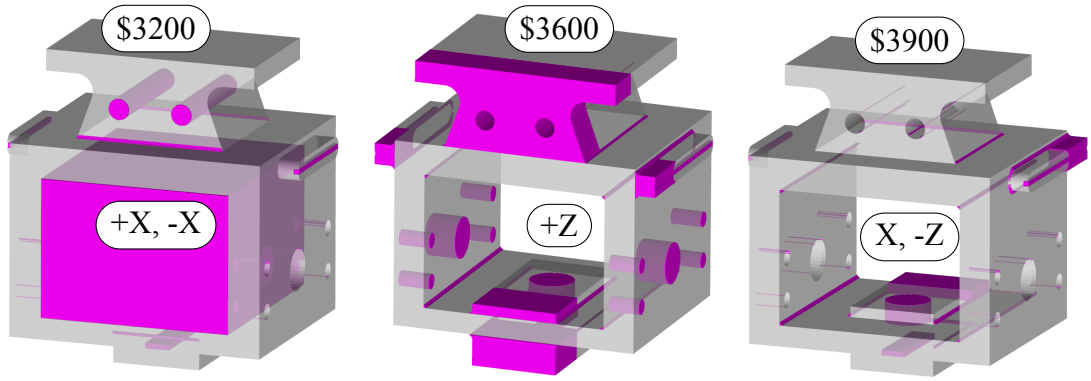

Figure 4.4: Three solutions from Pareto plot for part A with increasing cost and decreasing added volume. These solutions are located near to points “2”, “3”, and “4” from Fig. 4.2.

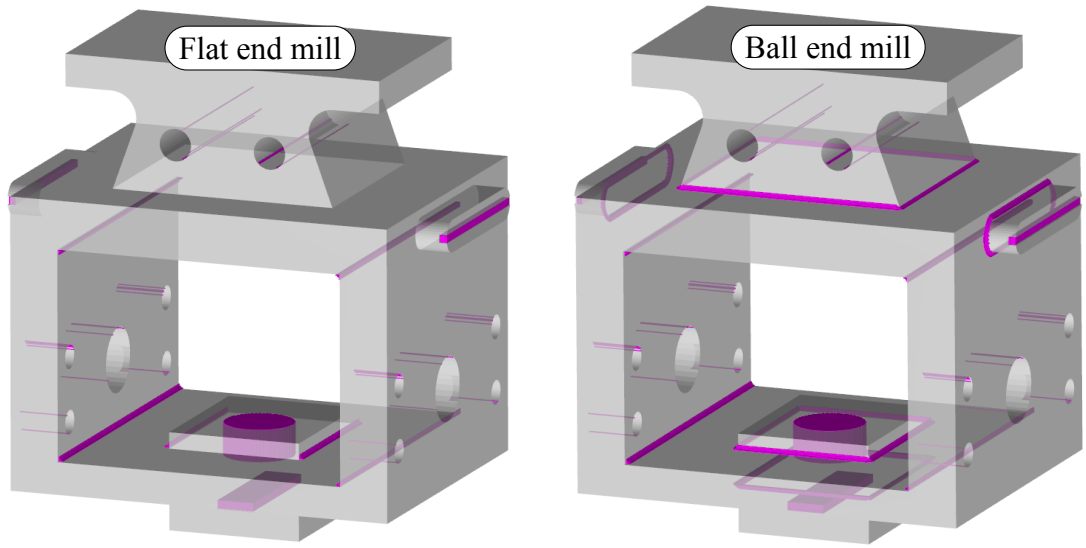

Figure 4.5: A flat end mill leaves fewer rounds in concave edges than a ball end mill, resulting in slightly better machinabiltiy for Part A.

4.2 Off-Axis Features: Part B

Part B (Pareto shown in Fig. 4.6) is a fairly simple part with only a few unique Pareto-optimal solutions. Three of these–located at points "1", "2", and "3" from the Pareto plot–are shown in Fig. 4.7. Given the simplicity of the part, one would expect it to be fully machinable with zero AV, but the discretized voxel operations leave small areas of unmachinable geometry in the solution at "3". The voxels need to be infinitesimally small for AV to truly reach zero. This part features off-axis holes that necessitate a setup direction which is not aligned with the part's cardinal axes. Consideration of the additional axis causes the search space to grow in size from 63 ($2^6 - 1$, only considering setups aligned with cardinal axes) solutions to 255 ($2^8 - 1$), which accounts for two additional setups lining up with the positive and negative directions of the off-axis drilled holes. Despite this, fewer total solutions (26) are evaluated by the search algorithm than for part A (63)–likely a result of the otherwise simple geometry on part B.

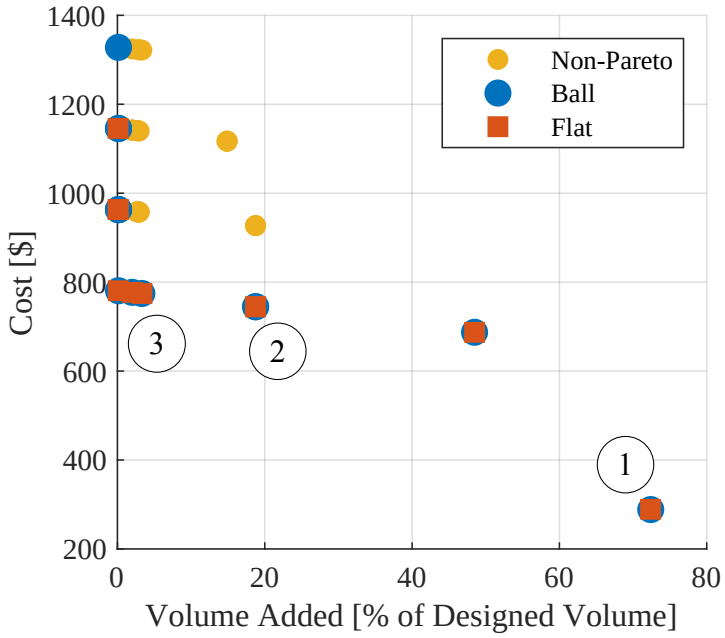

Figure 4.6: Pareto plot for Part B, which requires an off-axis machine setup. Note that there are still relatively few solutions.

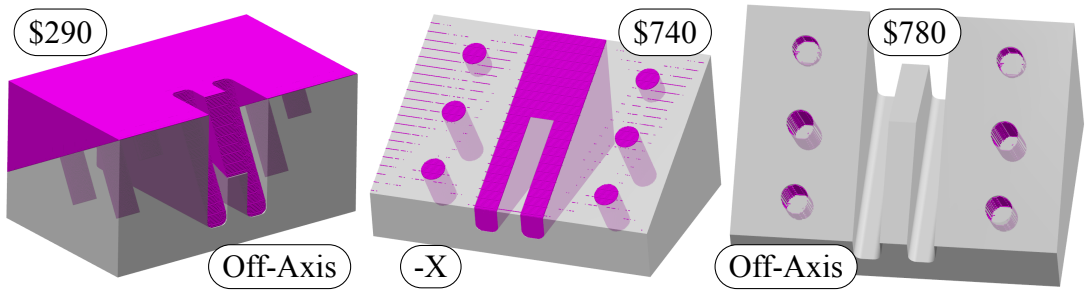

Figure 4.7: Three solutions from the Pareto plot for part B with increasing cost and decreasing added volume. These correspond to points "1", "2", and "3" from Fig. 4.6. In the solution approaching the as-designed shape, unmachinable material is left as artifacts of voxelization. This is a disadvantage of the voxelization approach, but it can be remedied with finer resolution voxels.

4.3 Topology Optimized: Part C

For the topology optimized part, C, the results show significant diminishing returns as additional machine setups are added. Near 10% AV, a cost of $450, and requiring only two setups–shown in Fig. 4.8–each successive machine setup removes comparatively little material but adds a significant amount of cost. Engineers working in industries where low mass has high importance, such as aerospace, may be more willing to include several added machine setups in order to reduce part weight. For others, the $450 part will be adequate so long as the part's functionality is maintained and the part still meets its engineering requirements. Near the cost axis, additional setups each remove less than 4 percent of volume while increasing cost approximately another $100 per setup.

This plot also best demonstrates striations (plot organized in linear bands) similarly found in the other Pareto plots. Of the two primary cost components–machining time and machine overhead–the overhead cost is dominated by the number of setups. Solutions with the same number of machine setups end up laying along the same line, and different numbers of setups form parallel lines on the Pareto plot. The Pareto-optimal solutions costing $450, $640, and $830 (using a ball end mill, and corresponding to circle solutions in Fig. 4.8) are shown in Fig. 4.9. A solution costing $150 is also Pareto-optimal, but a consequence of its low cost is high added volume (shown in Fig. 4.10). Beyond the lowest cost solution, the diagonal "legs" are well-defined. Notice how the contouring on the inner surfaces of the legs improves with more setups.

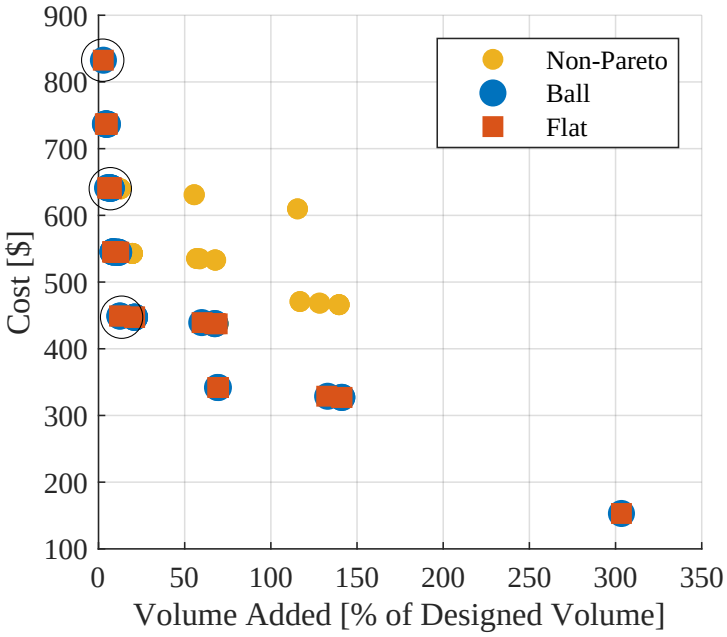

Figure 4.8: Pareto plot for topology optimized Part C. Note striation of solutions with different numbers of machining setups.

4.4 Key Takeaways

This straightforward view of tradeoff between cost and added volume can inform the engineer of difficult features to machine and of small or large geometry changes which reduce part cost. As in the other cases, by examining these modified geometries and associated costs, a design engineer can determine what part simplifications can be adopted to best decrease cost while maintaining part functionality. This may start by examining shapes from the Pareto that exhibit large decreases in added volume for specific machining setups, asymptotic behavior near the cost axis, or discontinuities in each additional machining setup.

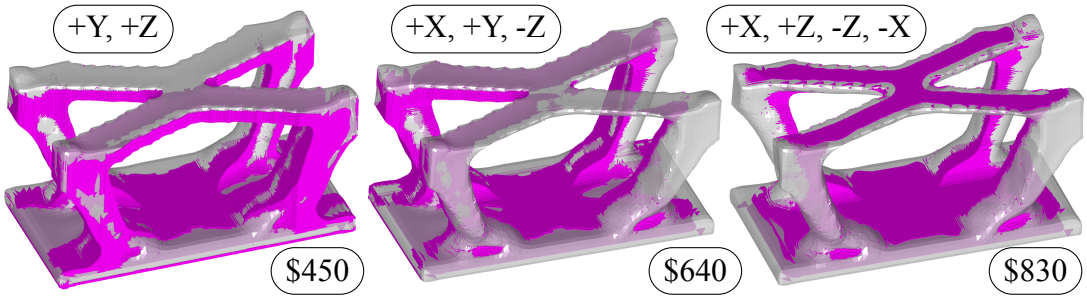

Figure 4.9: Topology optimized part C solutions which cost incrementally more to manufacture due to increased number of machining setups.

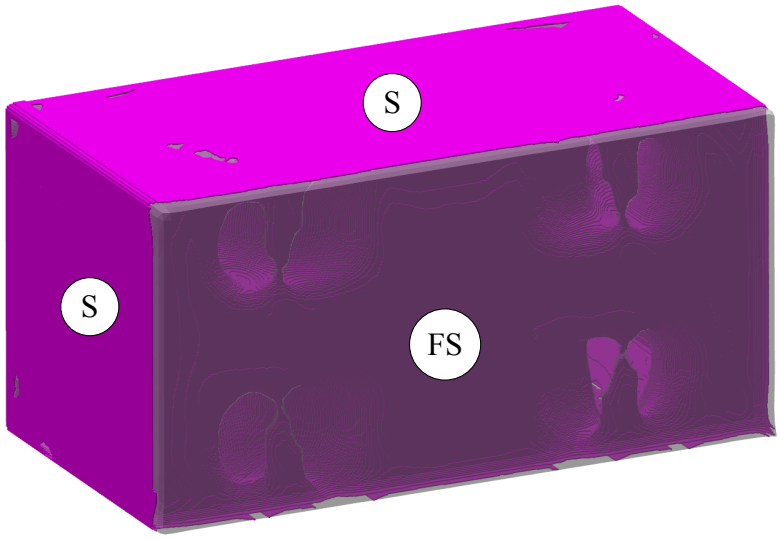

Figure 4.10: $150 solution for topology optimized Part C where very little machining is performed. The large flat surface (FS) is machined, as are the four adjacent sides (S).

Chapter 5: Methodology for Sub-Part Machining Plan Analysis

Following the machinability analysis of individual parts, cutting planes are introduced in an effort to gain access to unmachinable regions in parts and potentially reduce manufacturing cost by decreasing the amount of required stock material. Suitable cutting planes are determined automatically and the supplied part is sliced into multiple sub-parts. Those cutting planes might decrease overall bounding volume, expose previously unmachinable regions, or simply divide the part into two logical halves. Individual machinability analyses are performed on these sub-parts, and a composite machining plan is developed for each unique combination of sub-parts. The objective quantities (cost, volume, time, et cetera) can be directly compared between different composite machining plans and entire-part machining plans (no slicing performed). The methodology developed for this analysis builds directly upon those methods previously described in Chapter 3.

5.1 Sub-Part Search Space

The introduction of cutting planes causes the search space of machining plans to grow significantly. Whereas the space size for a single part machinability analysis–given in Eq. (3.1)–is $2^n - 1$, each sub-part now has its own search space of that same size. This is in addition to any machining operations performed after sub-parts are joined together.

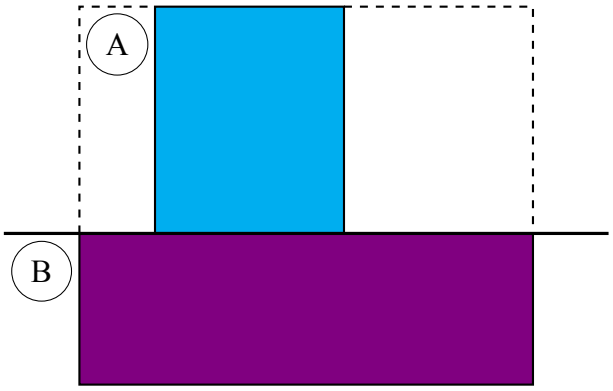

Figure 5.1: When a part is sliced–forming sub-parts A and B–A's stock material does not need to include the volumes bounded by dashed lines. This reduces overall material cost and waste, as well as machining cost.

Figure 5.1 shows an idealized part split by a single cutting plane into two sub-parts. Considering there may also be multiple cutting planes, the total number of candidate machining and joining plans to evaluate is found Eq. (5.1). The quantity $n_{m,k}$ is the number of machine setups considered for the k-sub-part of the m-cutting plane, and n_0 is the number of machining operations performed after sub-parts are joined together.

$$N = \sum_{m} \left(\left(\prod_{k} \left(2^{n_{m,k}} - 1 \right) \right) \left(2^{n_0} - 1 \right) \right) \tag{5.1}$$

Although this results in orders of magnitude more solutions than previously considered, many of these candidate solutions will prove unproductive by the same space reduction techniques employed when considering parts as a whole. In addition, new space reduction techniques are developed to aid in further culling the pool of candidate solutions. First and foremost, this analysis is currently limited to those cutting planes which produce only two sub-parts (i.e. a single left-hand solid and a single right-hand

solid). In the case where all sub-parts and the joined part share the same machine setups, estimating the overall size of the space becomes much simpler. Shown in Eq. (5.2), M is the total number number of cutting planes and n is still the number of unique machine setups (shared between sub-parts). A single cutting plane may now produce up to 250,047 candidate solutions, assuming the part requires only machine setups aligned with its cardinal axes.

$$N = M\left(2^n - 1\right)^3 \tag{5.2}$$

Certain sub-parts may not require any machining if they closely resemble available stock material shape and size, effectively reducing the exponent in Eq. (5.2) from 3 to 2. In the case where one sub-part requires no machining prior to joining (referred to as "pre-machining"), a single cutting plane will only produce 3,969 candidate solutions (still assuming only machine setups aligned with the part's cardinal axes). As a corollary to this, consider the case when both both sub-parts are fully machined. There is no longer a need for machining after these sub-parts are joined together, once again yielding 3,969 candidate solutions. When considering two additional off-axis directions, the number of possible solutions grows to 65,025.

5.2 Composite Machining Plan

There are many different ways to pair together individual sub-part machining analyses to create an overall manufacturing plan, referred to as a "composite machining plan".

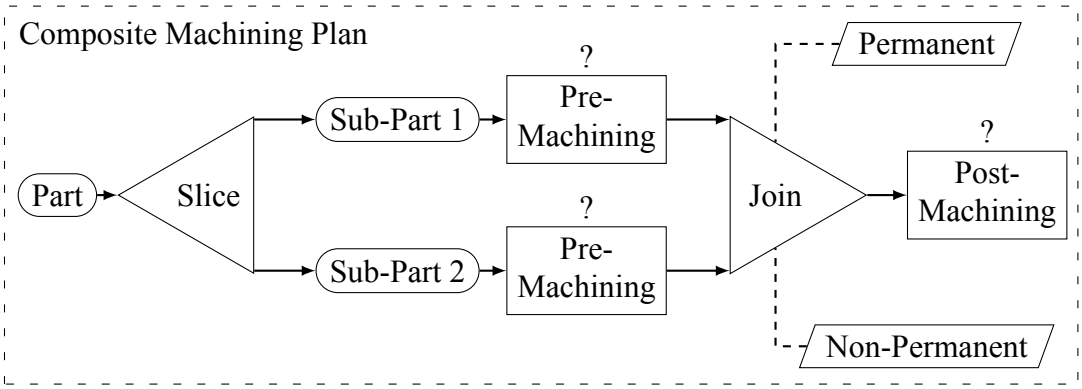

Figure 5.2: Flow-chart of the general sub-part machinability process. The design part is first sliced into multiple sub-parts, each of which can be pre-machined. The sub-parts are then joined together through either permanent or non-permanent methods, and the resulting part may be post-machined if necessary.

In the case of two sub-parts, Fig. 5.2 demonstrates the general process of performing a comprehensive machining plan optimization. The part is sliced into multiple sub-parts, sub-parts can be machined, and they are then joined together. This process can be either permanent (such as welding) or non-permanent (such as bolting). Finally, additional machining might be performed on the entire part.

One of the the simplest examples of this is taking taking two sub-parts, joining them together, and then performing all machining after they have been joined (referred to as "post-machining"). While this may not immediately seem interesting, this simple act of splitting the part in two could reduce the required stock material (and hence, waste) significantly, as demonstrated in Fig. 5.1. Another simple case is that where one or both sub-parts undergo pre-machining, but require no machining after they are joined together. The majority of candidate solutions can be characterized somewhere between

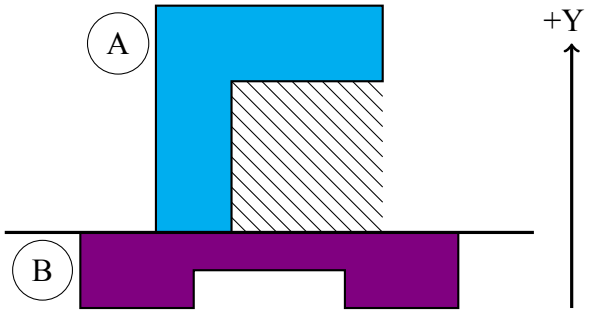

Figure 5.3: Material in the hatch-filled region (and belonging to sub-part A) cannot be machined away with post-machining in the +Y setup. The corresponding MMS–post-maching sub-part A in +Y direction–will not be created as it proves to be unproductive. Sub-part B might still utilize a +Y post-machining MMS, and a composite machining plan may still include +Y post-machining.

these two extremes, consisting of some pre-machining on individual sub-parts in addition to post-machining.

Although post-machining occurs after sub-parts are joined together, the methodology described in this thesis considers post-machining simultaneously with pre-machining for each sub-part. For each sub-part, maximum machinable shapes (MMSs) are created for both pre- and post-machining and selectively intersected together in a single machinability analysis. Those MMS corresponding to post-machining setups must take into account the geometric constraints of the rest of the part (i.e. other sub-part). Sub-part geometry may not be machinable with all post-machining setups (demonstrated in Fig. 5.3), and consequently the unproductive MMSs need not be created. Pre-machining MMSs can be created for each sub-part independently of the other, and unproductive MMSs are discarded (those which do not remove any material). A result of utilizing post-machining MMSs in each sub-part analysis is that only two distinct machining analyses need to be performed for each cutting plane–instead of three if post-machining were considered

separately. All voxel-based operations are performed at this stage on individual sub-parts.

After performing sub-part machining analyses, each sub-part has a set of unique machining plans which each contain some combination of pre- and post-machining setups. A single composite machining plan is formed with one machining plan for each sub-part. It is important to note that all sub-part machining plans forming a composite machining plan must contain the same combination of post-machining setups. An exception to this is when a post-machining operation is unproductive for a certain sub-part. The other sub-part may then contain that setup, illustrated in Fig. 5.3. No additional voxel operations are required beyond those already performed on each sub-part. Evaluating overall added volume simply involves taking a linear sum of the added volume for each sub-part. Cost is also evaluated as a linear sum with the inclusion of a joining penalty, discussed in the next section. The computationally-intensive sub-part machinability analyses are all performed at once. It then is computationally feasible to use those results to implicitly enumerate and evaluate all composite machining plans.

5.3 Sub-Part Joining Cost

The only new component factored into cost for any composite machining plan is the cost required for joining the sub-parts together. There are numerous ways sub-parts can be joined together, and which may be generalized with two categories: permanent (i.e. welding or chemical bonding) and non-permanent (i.e. bolting). The associated cost for a given joining operation may vary significantly between the two categories, and

even within each category depending on what different options are to be considered (i.e. friction versus arc welding). As a consequence of this wide variation, the additional cost due to joining is solely intended to be a size-dependant penalty. This avoids the need to develop complicated cost models of questionable accuracy. There could be two solutions with identical added volume and machining cost, while one requires slicing and joining of sub-parts and the other does not–i.e. is machined from a single piece of stock. The latter is a simpler solution, and inclusion of the joining penalty ensures that it is preferential over that solution involving sub-parts and joining.

Shown in Eq. (5.3), the cost is calculated as a sum of the machining costs for all individual sub-parts, C_i, in addition the newly introduced joining cost, C_{join}. Given by Eq. (5.4), the joining cost is approximated as being linearly proportional (through C_α and C_β) to both the area, A_{join}, and perimeter, P_{join}, being joined. and having some absolute minimum cost, C_γ. Additionally, there is a minimum cost, C_γ, independent of join area. This equation is further generalized for the possibility of performing sub-part machinability without required the sub-parts are joined together, in which case there is no joining cost.

$$C_{\text{total}} = C_{\text{join}} + \sum_i C_i \tag{5.3}$$

$$C_{\text{join}} = \begin{cases} C_\alpha A_{\text{join}} + C_\beta P_{\text{join}} + C_\gamma & \text{if joined} \\ 0 & \text{otherwise} \end{cases} \tag{5.4}$$

Chapter 6: Results for Sub-Part Machining Plan Analysis

Following the initial results on single part machinability analyses, this chapter presents an application of the sub-part machining plan optimization methodology to three different parts. The optimization for each part is performed with a ten-millimeter diameter flat end mill, and other machining parameters are identical to those reported in Chapter 4. The cost penalty associated with joining sub-parts is set to a base of $50 with an additional 2¢ per square millimeter of join area. Part A is used for this experiment, as well as two new parts. They are all of the same length scale, with minimum and maximum dimensions varying from 40 millimeters to 370 millimeters. Cutting planes to slice each part have been manually selected, although they can found automatically using methods developed by Massoni et al.[27].

Shown in Fig. 6.1, each part exhibits unique geometry features that test the proposed methods under various machining and slicing scenarios. Part A has a large internal void with protrusions in several different directions, as well as a small pocket which cannot be machined due to the overhang above it. Part D consists of base geometry with several extensions which significantly increase the overall stock volume. Part E is the result of a computer-aided topology optimization for a cantilever support, featuring internal voids and few prismatic features.

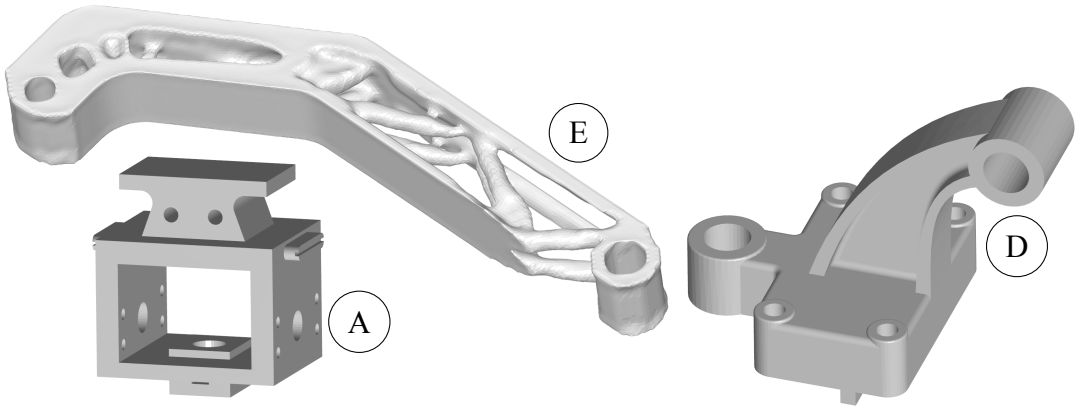

Figure 6.1: Sub-part machining plan test parts. A is the same test part used previously, containing unmachinable geometry; D features base geometry with extensions which significantly increases stock material size; E is another topology optimized part designed to support a cantilevered load.

6.1 Prismatic: Part A

The Pareto plot for this part is visually similar to that of the machinability analysis (Fig. 4.2), but with the inclusion of new sub-part solutions. Figure 6.2 shows the Pareto plot bounded to the lowest 10% added volume. Next to the circled "1" is the original solution–machined as a single monolithic part–with the least added volume. Slicing the part in two yields solutions with an added volume much closer to zero–near the circled "2" in the Pareto plot. However, these solutions are more expensive as a result of the necessary joining operation and negligible reduction in overall stock volume. The cost is increased from about $4100 to just over $4700 for the last two percent of added volume. These solutions still have a non-negligible amount of added volume, which is an artifact of the discretized voxel methods and discussed briefly in Section 4.2.

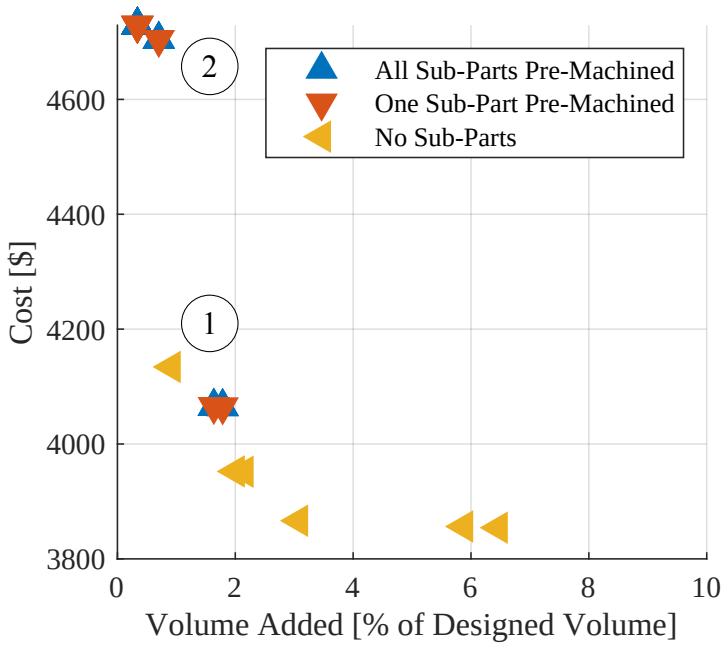

Figure 6.2: Pareto plot for sub-part machining plan results of Part A. Solutions involving slicing and pre-machining approach zero AV, but increase cost by about 15% ($600).

At this location near “2”, there are also overlapping solutions where some indicate both sub-parts are pre-machined and others only a single sub-part. Solutions belonging to the latter category only call for the sub-part containing the unmachinable region to be pre-machined. Provided two solutions have the same volume machined away and the same number of machine setups, their costs are also identical despite the different order of operations. This is intentional, as it lets the engineer independently evaluate the benefits of either pre-machining both sub-parts are only a single one. Depending on the type of joining utilized, post-machining may be preferential to clean up surfaces and

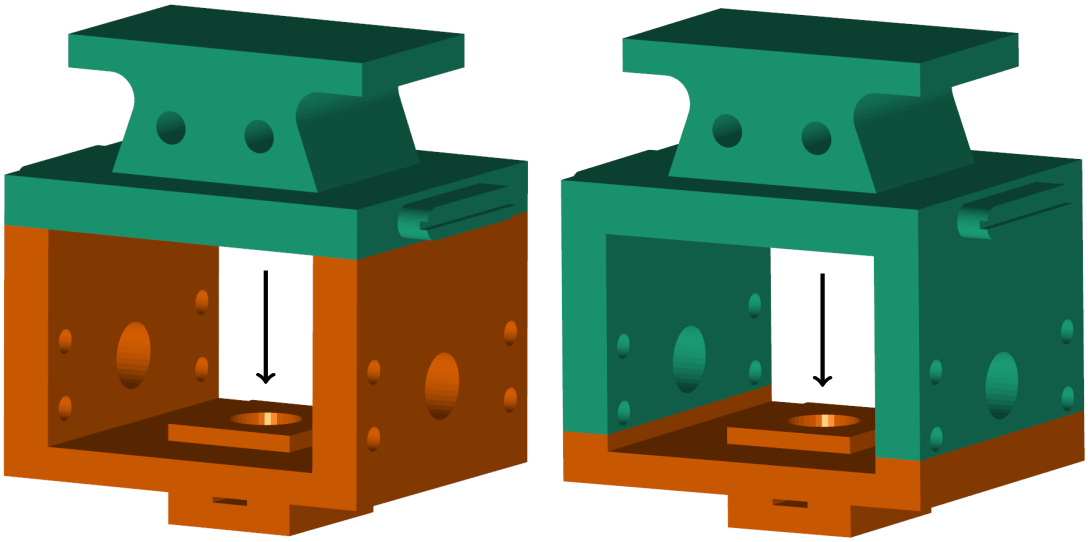

(a) (b)

Figure 6.3: Sub-parts for two different cutting planes used by test part A. Both cutting planes expose the unmachinable region (indicated by arrows) for removal with pre-machining of the lower (orange) sub-part. Within this part's Pareto plot (Fig. 6.2): (a) corresponds to the most volume-optimal solution group near circled "2", while (b) corresponds to the solution group immediately next to those, with slightly lower cost.

ensure features meet specified tolerances. On the other hand, smaller sub-parts might be fixtured with greater rigidity and milled in smaller–cheaper–machines.

Each distinct set of overlapping points near the circled "2" use a different cutting plane to slice the part, of which the resultant sub-parts are illustrated in Fig. 6.3. Both cutting planes share the same normal vector, but have different offsets along that direction. The unmachinable geometry for each is shown overlayed on the original part in Fig. 6.4. Note that the unmachinable region close to the geometric center of the part is now accessible and has been removed (solutions from Fig. 4.4 were unable to machine this area). Both solutions leave rounds in concave edges where the tool only passes over

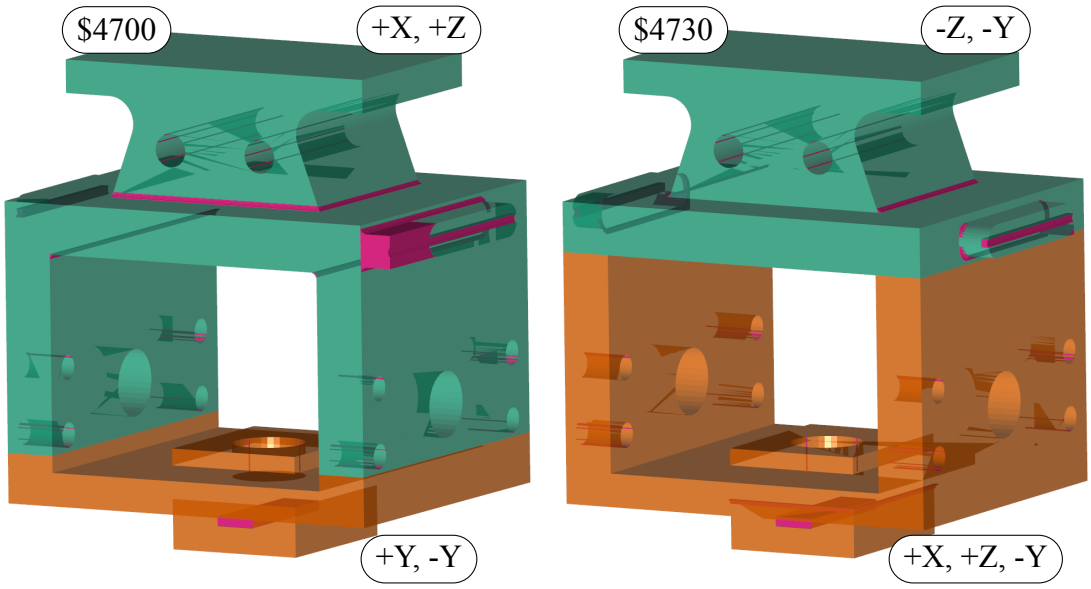

Figure 6.4: Machiniability results for two solutions groups of part A near circled "2" in Fig. 6.2. A single solution consisting of only pre-machining is selected to represent each group. Solution (b) has nearly zero added volume and negligibly higher cost–only 0.5%–than solution (a).

with a single setup. If undesirable, these can be eliminated altogether now that the part has been sliced and additional setups are capable of reaching these edges. The absolute reduction in volume for these additional setups was simply below the threshold for the machinability algorithm deemed "productive". Loosening the tolerance for minimum volume reduction per setup will allow such machine operations to populate candidate machining plans.

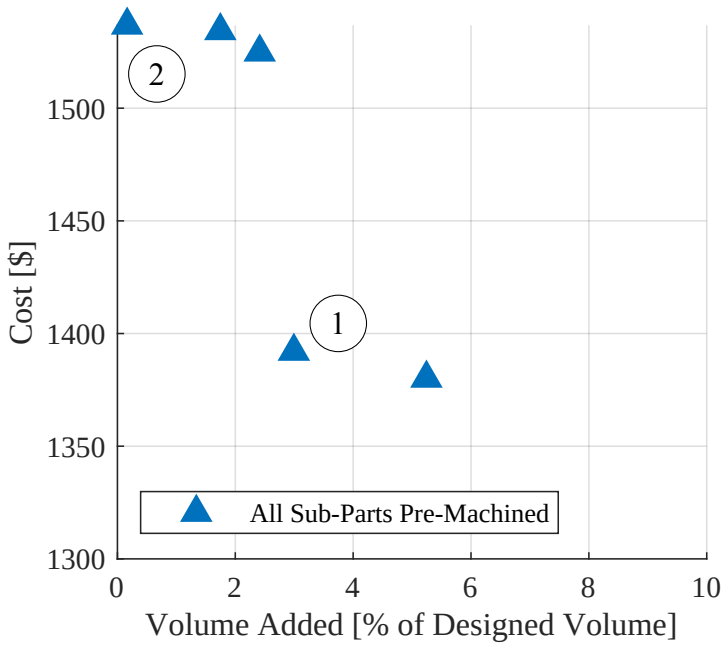

Figure 6.5: Pareto plot for sub-part machining plan results of Part D. All Pareto-optimal solutions (including those with more than 10% added volume) involve both sub-parts being fully pre-machined, and omit post-machining.

6.2 Prismatic: Part D

In comparison, the Pareto plot of part D is much simpler. Shown in Fig. 6.5, all solutions require that both sub-parts are fully pre-machined and undergo no post-machining. slicing the part yields such a large reduction in stock material–and therefore machining cost–that this offsets the cost penalty for joining the two sub-parts. All solutions on the Pareto share the same cutting plane, and the resultant sub-parts are shown in Fig. 6.6. This figure also shows the unmachinable geometry for solutions next to the circled “1” and “2”, respectively costing just under $1300 and just over $1550.

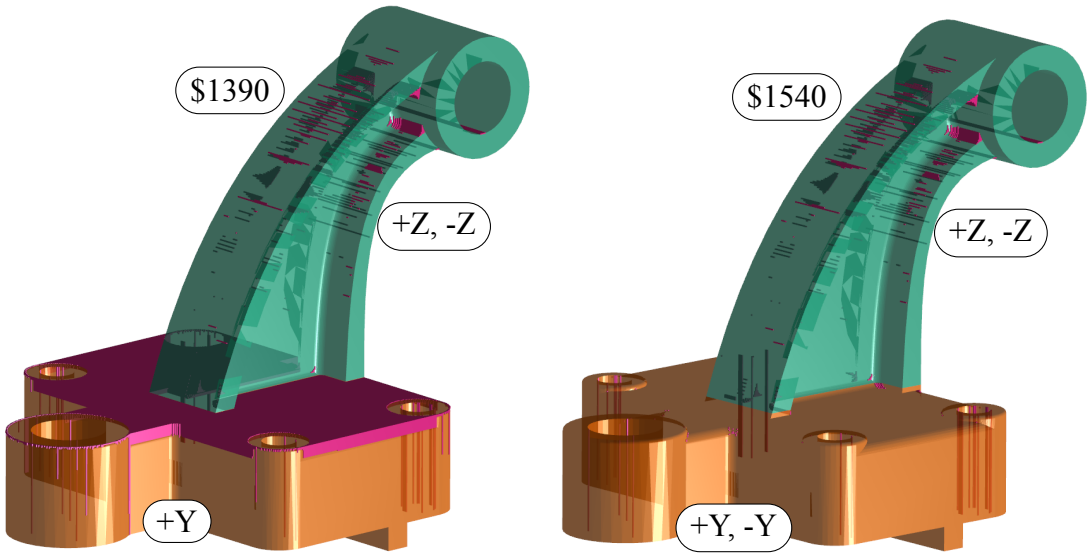

(a) (b)

Figure 6.6: The illustrated solutions (a) and (b) of part D correspond to points on the Pareto (Fig. 6.5) near the circled "1" and "2", respectively. While solution (a) has 3% added volume, it presents a nearly 10% cost savings over solution (b). Additionally, the added material does not appear to change the design of the part in any detrimental way.

Between both sub-parts, solution (a)–corresponding to "1" on the Pareto plot–only requires three machine setups. As a result, the top surface of the bottom (orange) sub-part is left unmachined and is raised upwards to the cutting plane or joining interface. Provided this alteration and 3% increase in added volume are acceptable changes, the overall part cost is reduced by $150 (or 10%) from that of fully machining the part. Solution (b)–corresponding to "2"–incorporates another pre-machining setup for the bottom (orange) sub-part to eliminate the remaining 3% added volume. Even considering this solution's $150 price jump over (a), it is still $640 (close to 30%) cheaper than the volume-optimal solution when machining as a single monolithic component.

6.3 Topology Optimized: Part E

Inspecting the Pareto plot for the second topology optimized part (shown in Fig. 6.7), there is a divide near 20% added volume where solutions with more added volume do not incorporate sub-parts. Alternatively, solutions with less added volume require that both sub-parts undergo pre-machining. Those few solutions where the part is sliced and pre-machined do not require that any post-machining is performed. Figure 6.8 shows machining plans corresponding to points “1” and “2” on the Pareto, labeled (a) and (b) respectively. The solution at (a) does not utilize slicing and needs only two machine setups, leading to a large amount of added volume (about 21%). The solution at (b) slices the part through its center with a Z-axis plane, and requires that each sub-part be machined with both machine setups normal to the cutting plane (+Z and -Z). The resulting halves are nominally mirror images of each other, and lend to a nearly 15% decrease in added volume over solution (a). Although this machining plan does present a 20% increase in cost, the machining comes closer to achieving the significantly reduced mass of that topology optimization provides for weight-sensitive parts.

6.4 Key Takeaways

Expanding upon the initial results presented in Chapter 4, design engineers are presented with clear treadeoffs between manufacturing complexity (or cost) and added volume. These tradeoffs can inform changes early in the design process to both reduce cost and improve machinability. The design engineer can determine if it necessary to manufacture multiple sub-parts and later join them together, and visualize geometric changes which

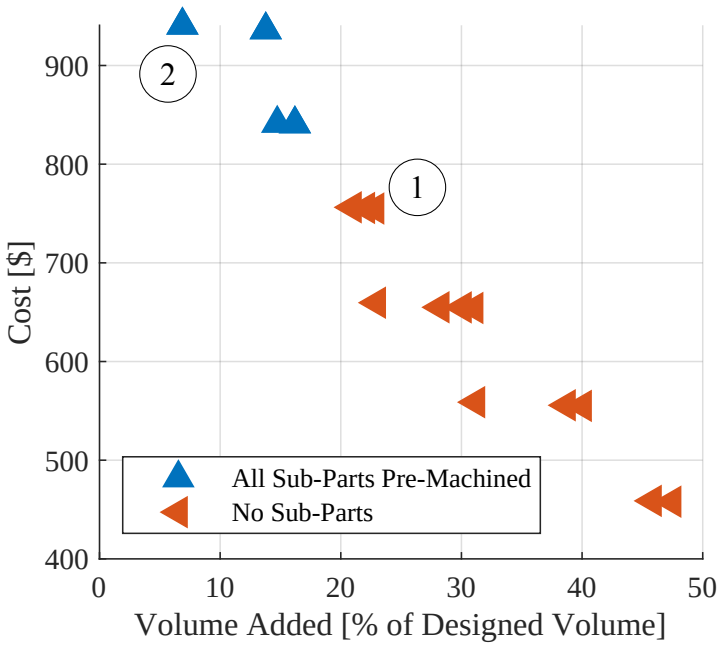

Figure 6.7: Pareto plot for sub-part machining plan results of topology optimized Part E. Due to the nature of the part, the volume-optimal solution still has nearly 10% added volume. These sub-part solutions do not require any post-machining steps.

simplify the machining process. These results show how slicing, pre-machining, and joining sub-parts together helps produce geometry much closer to the organic shapes which topology optimization algorithms are biased toward, when compared with machining a single monolithic part.

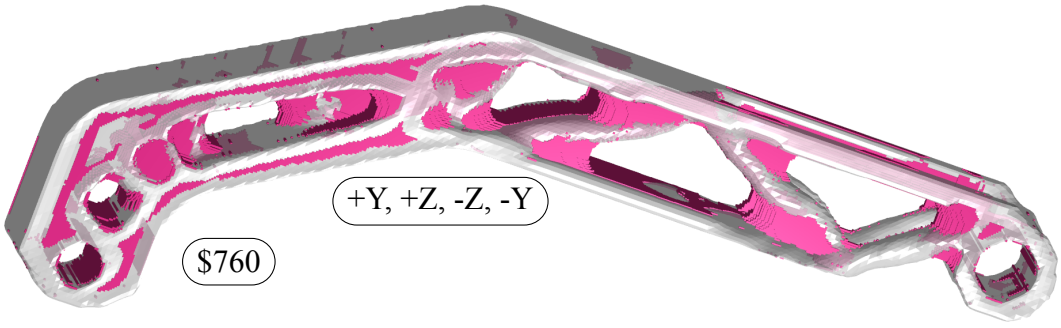

(a)

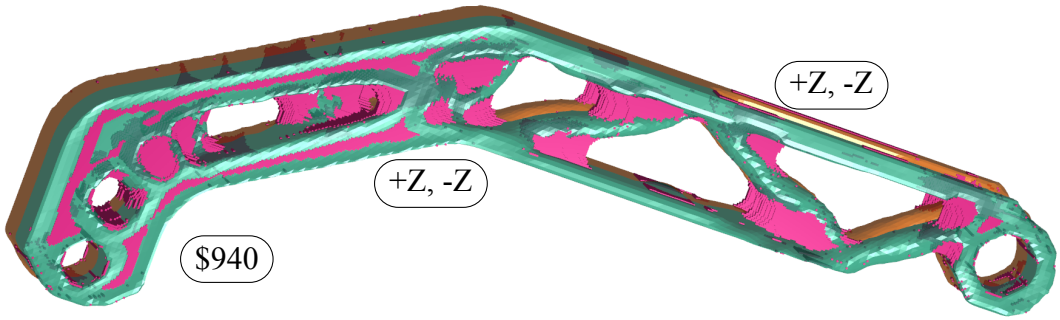

(b)

Figure 6.8: The cutting plane utilized by solution (b) of part E slices directly through the part's center along the Z-direction. All machining operations are aliened with this axis, and the two halves are nominally mirror images of each other. This solution corresponds to the point on the Pareto (Fig. 6.7) nearest the circled "2". Solution (a) does not incorporate a cutting plane, and corresponds to a point on the Pareto nearest the circled "1". Although (b) represents a nearly 15% decrease in added volume, it is visually similar to (a) and may not be worth the 20% increase in cost.

Chapter 7: Future Work

A natural extensions of the research presented in this thesis is to relax the constraints placed on cutting plane selection. Allowing there be multiple sub-parts on the same side of a cutting plane (and therefore more than two sub-parts for any cutting plane–is an immediate improvement to be made. There is also value in the ability to progressively join numerous sub-parts together, demonstrated in Fig. 7.1. Test part A will likely benefit from these additions to the algorithm, as it will then be possible to generate a machining plan which significantly reduces the volume of necessary stock material. In turn, material cost and machining cost both go down significantly.

The current approach for estimating machinability works well given the assumption of an infinite-length cutting tool, although in practice the cut depth is limited by several factors. Some additional factors include flute length, tool diameter, tool length extended from collet, and the amount of radial engagement in the cutting operation. A simple solution of these is to impose a global depth limit on the projection mask. Alternatively, voxels representing the collet and other tool-holding equipment can be added to the tool mask. This would ensure adequate clearance is maintained between parts and the milling machine.

There is currently no consideration for how a part or sub-part is fixtured within the machine. Using a vise to hold a part limits the amount of machining that can be performed in each setup, in this case by needing adequate clearance around the vise jaws.

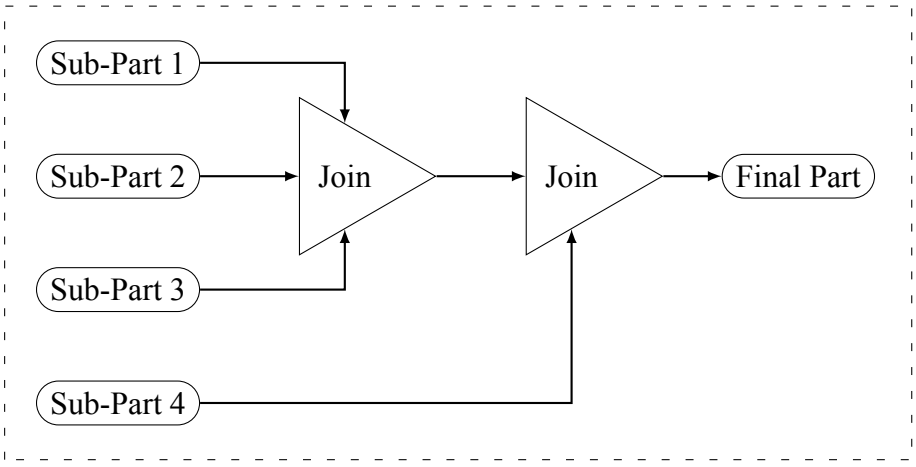

Figure 7.1: Example for how sub-parts might be progressively joined together. Machining steps are omitted from diagram, but may still be performed. Sub-parts 1, 2, and 3 are joined simultaneously. Their resultant part is then joined with sub-part 4, yielidng the final part geometry.

As the number of required setups increases, the regions held in the vise are more likely to be machined away without requiring a setup specifically for that purpose. Other fixture methods may require a distinct machining fixture per setup or a sacrificial fixture. Both cases will increase part cost by some amount that is not captured by the current cost models.

Additionally, all machining is assumed to be performed on 3-axis CNC milling machines. A logical expansion of the described methodology is to incorporate machining on 4- and 5- axis milling machines, as well CNC lathes. This greatly expands the search space, as a single setup performed on a multi-axis milling machine can achieve what would be a countless number of setups on a traditional 3-axis machine. Higher-axis machines will greatly improve the results for topology optimized parts, since the curved

surfaces that can only be accurately machined by simultaneously rotating and translating the part relative to the machine's spindle.

Finding additional setup directions not aligned with the part's cardinal axes has potential for improvement. Only cylinder axes are considered for these directions, and thresholds on the minimum radius and minimum area are imposed with little validation. There is also value in identifying large flat regions that are not parallel to any of a part's datum planes. New setups might be oriented both orthogonal and parallel to these surfaces.

Chapter 8: Conclusion

This thesis presented a methodology to perform featureless machinability and part decomposition analyses and cost estimation early in the design process. Tessellated and voxelized representations of a part are created, and potential machine setups are identified based on the part's cardinal axes and off-axis cylinders. Using automatically-identified or user-defined cutting planes, the part is sliced into multiple sub-parts which can be joined together after undergoing pre-machining. For each machine setup on each sub-part, the resultant geometry from the maximum possible machining is found. Similar geometry is found for each machine setup after sub-parts have been joined together.

Combinations of these solids are intersected together to find the final sub-part geometry for the corresponding set of machine setups. The machined geometry for each sub-part is unioned together, yielding the final part geometry after all machining and joining. Results are presented in the form design changes to the original part, as well as the estimated cost of those alternative designs and joining operations.

These methods were applied to several parts exhibiting different types of geometries, including unmachinable regions, prismatic off-axis geometry, large protrusions from base geometry, and topology optimized shapes. Pareto plots comparing cost and added volume help the design engineer evaluate a part's machinability and estimate production costs. The engineer can view geometry simplifications of topology optimized

parts machined monolithically, and can see the reduced machining cost as a result of those modifications.

Where the engineer cannot modify the already designed part or must minimize as much mass as is feasible, they are able to evaluate and estimate parts' machinability and cost when joined together from multiple sub-parts. All these analyses are usable early in the design process and provide results in a timely manner, giving the engineer has rapid feedback for how to improve parts' machinability while reducing their costs.

Bibliography

[1] J. Liu, A. T. Gaynor, S. Chen, Z. Kang, K. Suresh, A. Takezawa, L. Li, J. Kato, J. Tang, C. C. L. Wang, L. Cheng, X. Liang, and A. C. To, "Current and future trends in topology optimization for additive manufacturing," *Structural and Multidisciplinary Optimization*, vol. 57, pp. 2457–2483, 6 2018.

[2] M. Hoefer, N. Chen, and M. Frank, "Automated Manufacturability Analysis for Conceptual Design in New Product Development," in *Proceedings of the 2017 Industrial and Systems Engineering Research Conference* (K. Coerich, E. Cudney, and H. Nembhard, eds.), (Pittsburgh, PA), IISE, 2017.

[3] W. Kim and T. W. Simpson, "Toward Automated Design for Manufacturing Feedback," in *Advances in Production Management Systems. Sustainable Production and Service Supply Chains*, pp. 40–47, Berlin, Heidelberg: Springer, 2013.

[4] D. Jang, K. Kim, and J. Jung, "Voxel-Based Virtual Multi-Axis Machining," *The International Journal of Advanced Manufacturing Technology*, vol. 16, pp. 709–713, 8 2000.

[5] M. C. Frank, R. A. Wysk, and S. B. Joshi, "Determining Setup Orientations From the Visibility of Slice Geometry for Rapid Computer Numerically Controlled Machining," *Journal of Manufacturing Science and Engineering*, 2006.

[6] Y. Li and M. C. Frank, "Machinability Analysis for 3-Axis Flat End Milling," *Journal of Manufacturing Science and Engineering*, 2006.

[7] R. S. Lee, Y. H. Lin, M. Y. Tseng, and W. S. Wu, "Evaluation of workpiece orientation and configuration of multi-axis machine tool using visibility cone analysis," *International Journal of Computer Integrated Manufacturing*, vol. 23, no. 7, pp. 630–639, 2010.

[8] H. Samarghandy and Y. Li, "Detecting re-design area for increasing manufacturability of drilling and three-axis pocketing operations," *The International Journal of Advanced Manufacturing Technology*, vol. 69, pp. 337–349, 10 2013.

[9] C.-C. P. Chu and R. Gadh, "Feature-based approach for set-up minimization of process design from product design," *Computer-Aided Design*, vol. 28, pp. 321–332, 5 1996.

[10] S. K. Ong and L. Chew, "Evaluating the manufacturability of machined parts and their setup plans," *International Journal of Production Research*, vol. 38, pp. 2397–2415, 7 2000.

[11] W. Fu, A. A. Eftekharian, P. Radhakrishnan, M. I. Campbell, and C. Fritz, "A Graph Grammar Based Approach to Automated Manufacturing Planning," in *Volume 3: 38th Design Automation Conference, Parts A and B*, p. 77, ASME, 8 2012.

[12] S. Nelaturi, G. Burton, C. Fritz, and T. Kurtoglu, "Automatic spatial planning for machining operations," in *IEEE International Conference on Automation Science and Engineering*, 2015.

[13] S. Nelaturi, A. Rangarajan, C. Fritz, and T. Kurtoglu, "Automated fixture configuration for rapid manufacturing planning," *Computer-Aided Design*, vol. 46, pp. 160–169, 1 2014.

[14] M. Behandish, S. Nelaturi, and M. Allard, "Automated Process Planning for Turning: A Feature-Free Approach," in *Advances in Manufacturing Technology XXXII* (P. Thorvald and K. Case, eds.), (Skövde), pp. 45–50, IOS Press, 2018.

[15] R. Chan, K. R. Haapala, and M. I. Campbell, "Assessing Component Machinability Using Voxelized Solid Models," in *Volume 4: 23rd Design for Manufacturing and the Life Cycle Conference; 12th International Conference on Micro- and Nanosystems*, (Quebec City), p. V004T05A005, ASME, 8 2018.

[16] A. M. Mirzendehdel and K. Suresh, "A Pareto-Optimal Approach to Multimaterial Topology Optimization," *Journal of Mechanical Design*, vol. 137, p. 101701, 8 2015.

[17] G. Jared, M. Limage, I. Sherrin, and K. Swift, "Geometric reasoning and design for manufacture," *Computer-Aided Design*, vol. 26, pp. 528–536, 7 1994.

[18] S. K. Gupta, W. C. Regli, D. Das, and D. S. Nau, "Automated manufacturability analysis: A survey," *Research in Engineering Design*, vol. 9, pp. 168–190, 9 1997.

[19] J. Corbett and J. Crookall, "Design for Economic Manufacture," *CIRP Annals*, vol. 35, no. 1, pp. 93–97, 1986.

[20] G. Boothroyd and P. Radovanovic, "Estimating the Cost of Machined Components During the Conceptual Design of a Product," *CIRP Annals*, vol. 38, no. 1, pp. 157–160, 1989.

[21] T. S. Geiger and D. M. Dilts, "Automated design-to-cost: integrating costing into the design decision," *Computer-Aided Design*, vol. 28, pp. 423–438, 6 1996.

[22] J.-Y. Jung, "Manufacturing cost estimation for machined parts based on manufacturing features," *Journal of Intelligent Manufacturing*, vol. 13, no. 4, pp. 227–238, 2002.

[23] S. Das and A. Kanchanapiboon, "A multi-criteria model for evaluating design for manufacturability," *International Journal of Production Research*, vol. 49, pp. 1197–1217, 2 2011.

[24] aPriori Software, "Improving the Quality of Product Cost," Tech. Rep. March, aPriori Software, 2012.

[25] aPriori Software, "What Will My Design Cost to Produce?," tech. rep., aPriori Software, 2013.

[26] B. R. Massoni and M. I. Campbell, "A decomposition method for efficient manufacturing of complex parts," *Computer-Aided Design and Applications*, 2017.

[27] B. Massoni and M. I. Campbell, "Optimizing Cutting Planes for Advanced Joining and Additive Manufacturing," *Journal of Manufacturing Science and Engineering*, 2017.

[28] M. I. Campbell, "TVGL: Tessellation and Voxelization Geometry Library."

[29] C. Chan and S. Tan, "Determination of the minimum bounding box of an arbitrary solid: an iterative approach," *Computers & Structures*, vol. 79, pp. 1433–1449, 6 2001.

[30] N. Rafibakhsh and M. Campbell, "Hierarchical Fuzzy Primitive Surface Classification from Tessellated Solids for Defining Part-to-Part Removal Directions," *Journal of Computing and Information Science in Engineering*, vol. 18, no. 1, 2018.